BIOCHEMISTRY
including biophysical chemistry & molecular biology

Article

pubs.acs.org/biochemistry

Structural and Biochemical Analysis of the Phosphate Donor Specificity of the Polynucleotide Kinase Component of the Bacterial Pnkp•Hen1 RNA Repair System

Ushati Das, Li Kai Wang, Paul Smith, and Stewart Shuman*

Molecular Biology Program, Sloan-Kettering Institute, New York, New York 10065, United States

ABSTRACT: *Clostridium thermocellum* Pnkp is the end-healing and end-sealing subunit of a bacterial RNA repair system. *Cth*Pnkp is composed of three catalytic modules: an N-terminal 5′-OH polynucleotide kinase, a central 2′,3′ phosphatase, and a C-terminal ligase. The crystal structure of the kinase domain bound to ATP•Mg^{2+} revealed a rich network of ionic and hydrogen-bonding contacts to the α, β, and γ phosphates. By contrast, there are no enzymic contacts to the ribose and none with the adenine base other than a π–cation interaction with Arg116. Here we report that the enzyme uses ATP, GTP, CTP, UTP, or dATP as a phosphate donor for the 5′-OH kinase reaction. The enzyme also catalyzes the reverse reaction, in which a polynucleotide 5′-PO_4 group is transferred to ADP, GDP, CDP, UDP, or dADP to form the corresponding NTP. We report new crystal structures of the kinase in complexes with GTP, CTP, UTP, and dATP in which the respective nucleobases are stacked on Arg116 but make no other enzymic contacts. Mutating Arg116 to alanine elicits a 10-fold increase in K_m for ATP but has little effect on k_{cat}. These findings illuminate the basis for nonspecific donor nucleotide utilization by a P-loop phosphotransferase.

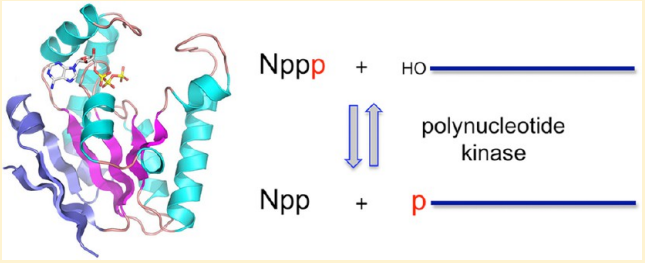

RNA repair is a mechanism to rectify RNA breaks incurred during RNA processing and cellular stress. RNA repair enzymes that seal 2′,3′-cyclic phosphate and 5′-OH ends are present in diverse taxa in all phylogenetic domains of life.[1,2] The Pnkp•Hen1 RNA repair system is encoded in an operon present in diverse bacteria from many phyla.[3−5] Pnkp is the end-healing and end-sealing component and comprises three catalytic domains: N-terminal kinase, central phosphatase, and C-terminal ligase.[3] The kinase catalyzes phosphoryl transfer to the 5′-OH RNA end. The phosphatase domain releases P_i from 2′-PO_4, 3′-PO_4, or 2′,3′-cyclic-PO_4 ribonucleotides.[6−9] The ligase domain has covalent adenylyltransferase activity and, in a 1:1 complex with the N-terminal half of the Hen1 protein, is an RNA ligase.[3,4,10,11] The C-terminal half of Hen1 is an autonomous Mn^{2+}-dependent 3′-terminal ribose 2′-*O*-methyltransferase that places a 2′-OCH_3 mark at the RNA repair junction prior to ligation and thereby protects the junction from recurrent damage.[4,5,12,13]

Crystal structures have been determined for each of the catalytic domains of *Clostridium thermocellum* Pnkp and Hen1.[10−12,14,15] The kinase, phosphatase, ligase, and 2′-*O*-methyltransferase modules are members of the P-loop phosphotransferase, binuclear metallophosphoesterase, covalent nucleotidyltransferase, and AdoMet-dependent methyltransferase enzyme superfamilies, respectively. In each case, the core superfamily fold is embellished by distinctive structural elements that either mediate protein−protein interactions or dictate substrate/cofactor specificity.

The N-terminal 170-amino acid segment of *Clostridium thermocellum* Pnkp is an autonomous polynucleotide kinase module. It phosphorylates 5′-OH single-stranded RNA or DNA substrates using ATP as the phosphate donor. We recently reported crystal structures of the kinase domain bound to ATP•Mg^{2+} and ADP•Mg^{2+}, reflective of substrate and product complexes, respectively.[14] The ATP donor is bound within a crescent-shaped groove formed by the P-loop (^{15}GSSGSGKST^{23}) and an overlying lid composed of helices α6 and α7 and the connecting ^{120}RTDRQVE^{126} peptide (Figure 1A). The ATP α and β phosphates are engaged by a network of hydrogen bonds from Thr23 and the P-loop main-chain amides; the γ phosphate is anchored by the lid residues Arg120 and Arg123 and the P-loop Ser17. The P-loop lysine (Lys21) and the catalytic Mg^{2+} bridge the ATP β and γ phosphates. The P-loop serine (Ser22) is the sole enzymic constituent of the octahedral metal coordination complex, which also includes nonbridging β and γ phosphate oxygens of ATP and three waters (Figure 1A). A secondary shell of atomic contacts to the metal-bound waters in the metal complex includes the Asp38 and Asp78 side chains. Structure-guided mutational analysis underscored the essential contributions of Lys21 and Ser22 in the ATP donor site and Asp38 and Arg41 in the putative phosphoacceptor site. Our studies suggested a catalytic mechanism whereby Asp38 (as general base) activates

Received: April 2, 2013
Revised: May 2, 2013
Published: May 31, 2013

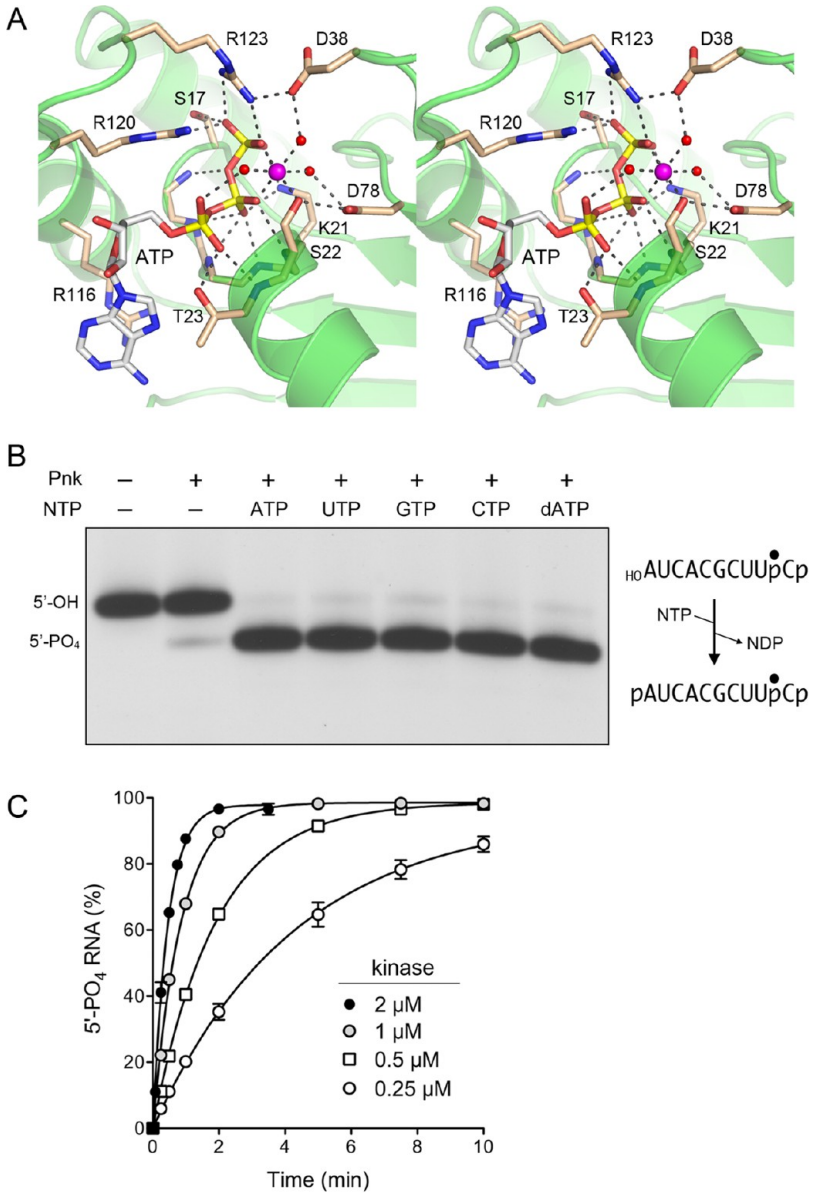

Figure 1. NTP donor specificity of the kinase reaction. (A) Stereoview of the phosphate donor site of the A protomer of the kinase•ATP•Mg^{2+} substrate complex (pdb 4GP7). Amino acids and ATP are shown as stick models with beige and gray carbons, respectively. Mg^{2+} is depicted by a magenta sphere in the center of an octahedral coordination complex. Waters in the metal coordination complex are denoted by red spheres. Atomic contacts are indicated by dashed lines. (B) Kinase reactions were performed as described in Experimental Procedures. The reaction mixtures included 100 μM NTPs as specified, 0.05 μM 10-mer $_{HO}$RNAp phosphoacceptor (5′-$_{HO}$AUCACGCUU**p**Cp) labeled with ^{32}P at the penultimate phosphate, and 0.25 μM kinase (Pnk +). The ^{32}P-labeled RNAs were resolved by PAGE and visualized by autoradiography. The radiolabeled species corresponding to the 5′-OH substrate RNA and the 5′-PO_4 product RNA are indicated at left. (C) Kinetics. Reaction mixtures containing 50 mM Tris-HCl (pH 7.0), 10 mM $MgCl_2$, 5 mM DTT, 100 μM ATP, 0.05 μM ^{32}P-labeled 10-mer $_{HO}$RNAp phosphoacceptor, and 0.25, 0.5, 1.0, or 2.0 μM kinase as indicated were incubated at 45 °C. Aliquots (10 μL) were withdrawn at times specified and quenched immediately with formamide/EDTA. The time 0 samples were withdrawn prior to adding kinase. Product formation is plotted versus reaction time. Each datum is the average of three independent time course experiments (±SEM). The data were fit by nonlinear regression to a one-phase association function in Prism.

the polynucleotide 5′-OH for its nucleophilic attack on the γ phosphorus and Lys21 and Mg^{2+} stabilize the transition state.[14]

It is notable that there are no protein contacts to the ATP ribose sugar or to the nitrogen atoms of the adenine nucleobase. The sole protein interaction with adenine is via a π−cation stack on the Arg116 side chain of the lid (Figure 1A). This situation contrasts with many other P-loop enzymes, especially helicases, that make hydrogen bonds to the adenine N6 and N7 atoms via a conserved glutamine side chain that confers specificity for ATP or dATP as the phosphohydrolase substrate.[16,17] Prompted by the *Cth*Pnkp kinase•ATP structure, we investigate the donor specificity of this exemplary bacterial RNA repair enzyme and probe the contributions of the Arg116 side chain. We report that the kinase is nonspecific with respect to the nucleotide substrate, being adept at phosphoryl transfer, in the forward and reverse direction, to guanosine, cytidine, uridine, and deoxyadenosine nucleotides. We also determine new atomic structures of the kinase in complexes with Mg^{2+} and GTP, CTP, UTP, and dATP that reveal, in every case, an *anti* nucleoside conformation and an Arg116•nucleobase π−

dx.doi.org/10.1021/bi400412x | *Biochemistry* 2013, 52, 4734−4743

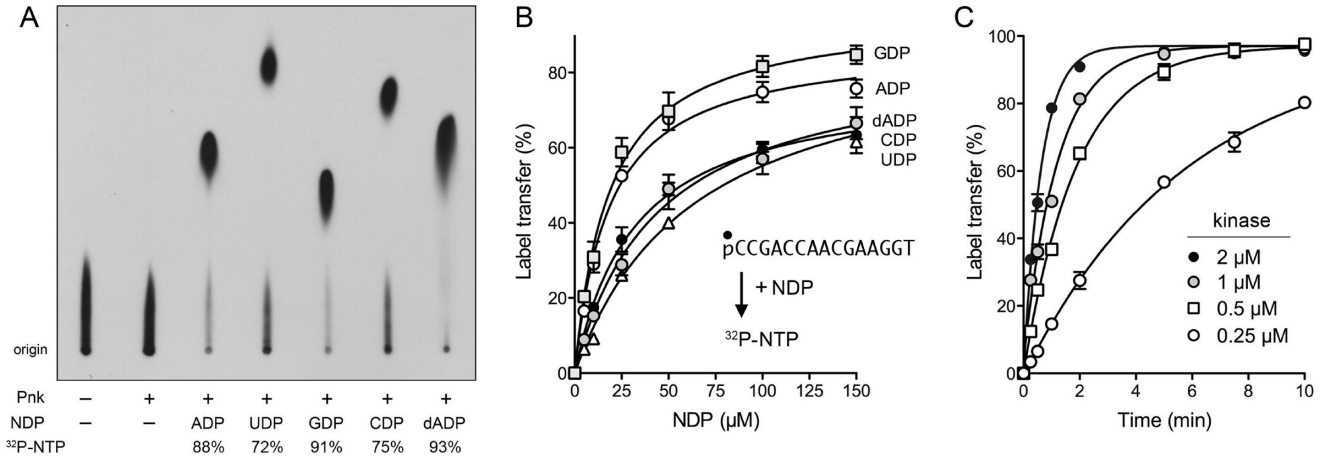

Figure 2. NDP acceptor specificity of the reverse kinase reaction. (A) Reverse kinase reactions were performed as described in Experimental Procedures. The reaction mixtures included 0.1 μM 5′-^{32}P-labeled 15-mer DNA oligonucleotide (pCCGACCAACGAAGGT), 100 μM ADP, UDP, GDP, CDP, or dADP as specified, and 0.25 μM kinase (Pnk+). The radiolabeled products were resolved by TLC and visualized by autoradiography, which showed label transfer from the ^{32}P-DNA oligonucleotide to the added NDP acceptor to form the respective ^{32}P-labeled NTPs. The extents of label transfer to the NDPs are indicated below the lanes. (B) NDP dependence. Reaction mixtures (10 μL) containing 50 mM Tris-HCl (pH 7.0), 10 mM $MgCl_2$, 5 mM DTT, 0.1 μM 5′-^{32}P-labeled 15-mer oligonucleotide, 0.125 μM kinase, and NDP as indicated were incubated at 45 °C for 30 min. The products were analyzed by TLC. The extent of ^{32}P-NTP formation is plotted as a function of NDP concentration. Each datum is the average of three independent titration experiments (±SEM). Nonlinear regression fitting of the data to the Michaelis–Menten equation was performed in Prism. (C) Kinetics. Reaction mixtures containing 50 mM Tris-HCl (pH 7.0), 10 mM $MgCl_2$, 5 mM DTT, 100 μM ADP, 0.1 μM of a 15-mer 5′-^{32}P labeled 15-mer oligonucleotide, and 0.25, 0.5, 1.0, or 2.0 μM kinase as indicated were incubated at 45 °C. Aliquots (10 μL) were withdrawn at times specified and quenched immediately with formic acid. The time 0 sample was withdrawn prior to adding kinase. The products were analyzed by TLC. The extents of label transfer to form ^{32}P-ATP are plotted versus reaction time. Each datum is the average of three independent time course experiments (±SEM). The data were fit by nonlinear regression to a one-phase association function in Prism.

cation stack. We compare and contrast the nucleotide binding modes of polynucleotide kinases from diverse taxa.

EXPERIMENTAL PROCEDURES

Kinase Purification and Mutagenesis. The pET28b-Smt3*Cth*Pnkp-(1–170) expression plasmid encoding the kinase domain was described previously.[14] Missense mutations R116A, R120A, R123A, and R120A–R123A were introduced into the expression vector by the two-stage PCR-based overlap extension method. The Pnkp inserts were sequenced to confirm the presence of the desired mutation and the absence of unwanted coding changes. The plasmids were transformed into *Escherichia coli* BL21(DE3). Recombinant protein production was induced by adjusting exponentially growing cultures (1 L) to 0.3 mM IPTG and incubating them at 17 °C for 15 h with continuous shaking. Cells were harvested by centrifugation and stored at −80 °C. All subsequent procedures were performed at 4 °C. Thawed cell pellets were resuspended in 50 mL of lysis buffer (50 mM Tris-HCl, pH 7.5, 1.2 M NaCl, 25 mM imidazole, 10% glycerol). Lysozyme and Triton X-100 were added to final concentrations of 1 mg/mL and 0.2%, respectively; one protease inhibitor tablet (Roche) was then added. The lysates were sonicated to reduce viscosity, and insoluble material was removed by centrifugation for 1 h at 14400 rpm in a Sorvall SLA-1500 rotor. The soluble extracts were applied to 4 mL columns of Ni-nitriloacetic acid agarose (Qiagen) that had been equilibrated in buffer A (50 mM Tris-HCl, pH 7.5, 200 mM NaCl, 10% glycerol). The columns were washed with 12 mL of buffer A and 12 mL of 100 mM imidazole in buffer A. The His-tagged *Cth*Pnkp proteins were recovered by serial stepwise elution with 200 mM imidazole and 300 mM imidazole in buffer A. The elution profiles were monitored by SDS-PAGE. Peak *Cth*Pnkp-containing fractions were pooled and supplemented with Smt3-specific protease Ulp1 (protein: Ulp1 in a molar ratio of 50:1), and the mixture was dialyzed overnight against 4 L of buffer B (50 mM Tris-HCl, pH 7.5, 100 mM NaCl, 10% glycerol). The tag-free *Cth*Pnkp protein was separated from the cleaved His_{10}Smt3 tag by a second round of Ni-agarose chromatography, during which *Cth*Pnkp was recovered in the flow-through fraction. The Ni-agarose *Cth*Pnkp-(1–170) preparations were used for the assays of kinase-specific activity reported in Figure 6. For further purification of wild-type *Cth*Pnkp-(1–170) and the R116A mutant, the Ni-agarose preparations were adjusted to 10 mM EDTA, concentrated by centrifugal ultrafiltration, and gel-filtered through a column of Superdex-200 equilibrated in 50 mM Tris-HCl pH 7.5, 100 mM NaCl, 10% glycerol, 1 mM DTT, 1 mM EDTA. The enzyme preparations were stored at −80 °C. Protein concentrations were determined by using the BioRad dye reagent with bovine serum albumin as the standard.

Assay of the NTP Donor Specificity of the Kinase Reaction. Reaction mixtures (10 μL) containing 50 mM Tris-HCl (pH 7.0), 10 mM $MgCl_2$, 5 mM DTT, 100 μM NTPs as specified, 0.05 μM of a 10-mer $_{HO}$RNAp phosphoacceptor (5′-$_{HO}$AUCACGCUU**p**Cp) labeled with ^{32}P at the penultimate phosphate (prepared as described[20]), and 0.25 μM kinase were incubated at 45 °C for 30 min. The reactions were initiated by adding enzyme to reaction mixtures prewarmed to 45 °C and quenched by adding an equal volume of 90% formamide, 50 mM EDTA, and 0.01% bromophenol blue/xylene cyanol. The mixtures were analyzed by electrophoresis (at 55 W constant power) through a 40 cm 20% polyacrylamide gel containing 8 M urea in 45 mM Tris-borate, 1.2 mM EDTA. The ^{32}P-labeled RNAs were visualized by autoradiography, which showed that the $_{HO}$RNAp substrate was separated from the faster migrating pRNAp product (Figure 1B). The extent of RNA phosphorylation was determined by scanning the gel with a FujiFilm

dx.doi.org/10.1021/bi400412x | *Biochemistry* 2013, 52, 4734–4743

Table 1. Crystallographic Data and Refinement Statistics[a]

	UTP	GTP	CTP	dATP
space group	$P2_12_12_1$	$P2_12_12_1$	$P2_12_12_1$	$P2_12_12_1$
unit cell dimensions (Å) at 130 K	a = 45.31	a = 45.31	a = 45.31	a = 45.31
	b = 66.78	b = 66.78	b = 66.78	b = 66.78
	c = 119.55	c = 119.55	c = 119.55	c = 119.55
diffraction data quality				
resolution (Å)	46.1−2.03 (2.08−2.03)	39.6−2.14 (2.26−2.14)	58.0−2.48 (2.58−2.48)	45.5−2.02 (2.07−2.02)
radiation source	NSLS X25	NSLS X25	NSLS X25	NSLS X25
wavelength, Å	1.10	1.10	1.10	1.10
processing software	Mosflm/Scala	Mosflm/Scala	Mosflm/Scala	Mosflm/Scala
R_{sym},[b] %	5.9 (19.9)	9.1 (18.6)	7.6 (18.8)	4.8 (15.4)
unique reflections	24709 (1787)	20889 (2998)	13156 (1445)	24363 (1760)
mean redundancy	6.1 (5.6)	11.9 (12.0)	6.0 (6.2)	5.9 (5.2)
completeness, %	100.0 (100.0)	100.0 (100.0)	100.0 (100.0)	99.7 (99.2)
mean $I/\sigma I$	17.7 (7.3)	17.4 (9.8)	17.4 (8.4)	22.5 (9.6)
refinement and model statistics ($F > 1.34\sigma F$)				
resolution (Å)	44.5−2.03 (2.08−2.03)	37.5−2.14 (2.20−2.14)	44.5−2.49 (2.62−2.49)	44.5−2.02 (2.07−2.02)
completeness, %	99.8 (98.6)	99.8 (97.0)	98.8 (92.0)	98.9 (90.2)
R_{free}[c]/R_{work}, %	22.4/17.0 (27.3/19.4)	20.4/16.8 (21.0/16.2)	22.7/18.1 (28.7/20.2)	21.4/15.3 (23.7/15.1)
RMSD bonds/angles	0.009 Å/1.26°	0.005 Å/1.00°	0.006 Å/1.09°	0.010 Å/1.28°
Ramachandran plot	99.1% favored, no outliers	99.7% favored, no outliers	99.7% favored, no outliers	98.8% favored, no outliers
B-factors, Å^2				
Wilson/overall	22.9/29.2	21.9/24.3	27.9/36.4	22.0/27.2
protein/NTP				
protomer A	29.1/31.3	23.5/26.0	35.7/31.9	25.4/26.1
protomer B	29.6/20.7	24.7/24.4	37.6/33.6	28.0/24.6
mean TLS anisotropy[d]			0.67 over 7 groups	
model contents				
protein residues	342	342	341	342
heteroatoms	2 UTP, 2 Mg^{2+}, 1 Na^+	2 GTP, 2 Mg^{2+}	2 CTP, 2 Mg^{2+}	2 dATP, 2 Mg^{2+}, 1 Na^+
waters	266	180	126	279
PDB ID	4JST	4JSY	4JT2	4JT4

[a]Standard definitions are used for all parameters. Figures in parentheses refer to data in the highest resolution bin. The refinement and geometric statistics come from PHENIX. [b]R_{sym} output as R_{merge} by SCALA. [c]R_{free} sets consisted of 8% data chosen at random against which structures were not refined. [d]TLS refinement was carried out only for the kinase•CTP complex.

BAS-2500 imager and quantifying pRNAp/(pRNAp + $_{HO}$RNAp).

Assay of the NDP Acceptor Specificity of the Reverse Kinase Reaction. Reaction mixtures (10 μL) containing 50 mM Tris-HCl (pH 7.0), 10 mM $MgCl_2$, 5 mM DTT, 0.1 μM of a 5′-^{32}P labeled 15-mer DNA oligonucleotide (pCCGACCAACGAAGGT), 100 μM ADP, UDP, GDP, CDP, or dADP as specified, and 0.25 μM kinase were incubated at 45 °C for 30 min. The reactions were quenched by adding 2 μL of 5 M formic acid. An aliquot (5 μL) of each reaction mixture was applied to a polyethyleneimine−cellulose TLC plate and then overlaid with 10 nmol of the corresponding cold NTP standards. Ascending TLC was performed with 0.45 M $(NH_4)_2SO_4$. The radiolabeled products were visualized by autoradiography (see Figure 2A). Reverse kinase activity was evinced by label transfer from the ^{32}P-DNA oligonucleotide (pDNA, located at and trailing from the chromatographic origin) to the added NDP acceptor to form the respective ^{32}P-labeled NTPs that comigrated with the cold NTP standards that were located by UV autofluorescence. The extents of label transfer to the NDPs were determined by scanning the plate with a FujiFilm BAS-2500 imager and quantifying NTP/(NTP + pDNA).

Kinase Assay by Label Transfer from ATP to a 5′-OH Oligonucleotide Acceptor. Reaction mixtures (10 μL) containing 50 mM Tris-HCl (pH 7.0), 10 mM $MgCl_2$, 5 mM DTT, 100 μM [γ^{32}P]ATP, 60 pmol of a 15-mer 5′-OH DNA oligonucleotide phosphoacceptor ($_{HO}$CCGACCAACGAAGGT), and wild-type or mutant kinase as specified were incubated for 30 min at 45 °C. The reactions were quenched by adding an equal volume of 90% formamide, 50 mM EDTA, and 0.01% bromophenol blue/xylene cyanol, and the mixtures were analyzed by electrophoresis (at 7 W constant power) through a 15 cm 20% polyacrylamide gel containing 8 M urea in 45 mM Tris-borate and 1.2 mM EDTA. The ^{32}P-labeled DNAs were visualized and quantified by scanning the gel with a FujiFilm BAS-2500 imager.

Crystallization, Diffraction Data Collection, and Structure Determination. The SeMet-kinase preparation of *Cth*Pnkp-(1−170)-V44M-L137M described previously[14] was concentrated to 7.8 mg/mL and adjusted to 2 mM GTP, CTP, UTP, or dATP plus 10 mM $MgCl_2$ and incubated for 10 min before aliquots of the protein solution (2 μL) were mixed on a coverslip with an equal volume of precipitant solution containing 100 mM sodium citrate, pH 5.6, 100 mM $MgCl_2$, and 16−18% (v/v) PEG-3350. Crystals were grown at 22 °C by hanging drop vapor diffusion against a reservoir of the same precipitant solution. Single crystals were transferred to a solution containing 100 mM sodium citrate, pH 5.6, 2 mM NTP, 100 mM $MgCl_2$, 16−18% PEG-3350, and 15% glycerol

dx.doi.org/10.1021/bi400412x | *Biochemistry* 2013, 52, 4734−4743

prior to freezing the crystals in liquid nitrogen. Diffraction data for each *Cth*Pnkp•NTP•Mg^{2+} complex were collected at NSLS beamline X25 equipped with a Pilatus 6 M detector in 370 continuous increments of 0.5° each. The data were integrated and reduced with MOSFLM and SCALA. Diffraction statistics are compiled in Table 1. The kinase•NTP•Mg^{2+} crystals were in space group $P2_12_12_1$, had two protomers per asymmetric unit, and were isomorphous with the SeMet kinase•ATP•Mg^{2+} crystals reported previously.[14] Structures of kinase•GTP•Mg^{2+}, kinase•UTP•Mg^{2+}, and kinase•dATP•Mg^{2+} complexes at 2.02−2.14 Å resolution and kinase•CTP•Mg^{2+} at 2.5 Å resolution were determined by refinement of the diffraction data against the SeMet kinase•ATP•Mg^{2+} structure (PDB ID 4GP7) from which ATP•Mg^{2+} and waters had been removed. The NTPs and Mg^{2+} were then modeled into the F_o-F_c maps of the respective active sites. The models were iteratively rebuilt by hand in COOT[18] and refined in PHENIX.[19] NCS restraints and TLS B-factor refinements in PHENIX were carried out only for the kinase•CTP complex. The final models had excellent geometry, no Ramachandran outliers, and no large F_o-F_c difference Fourier peaks (Table 1).

RESULTS

NTP Donor Specificity of *Cth*Pnkp Kinase. The kinase activity of the Pnkp protein was assayed by the transfer of phosphate from cold NTPs to a 10-mer 5′-OH RNA acceptor with a 3′-PO_4 terminus and a single ^{32}P-radiolabel between the 3′-terminal and penultimate nucleosides (Figure 1B). In the presence of kinase and ATP, 98% of the input $_{HO}$RNAp strand was converted to a pRNAp product. When ATP was omitted, only 2.7% of the RNA substrate was phosphorylated, reflecting the presence of a trace level of NTP-bound kinase in the enzyme preparation. From the extent of ATP-independent product formation, we calculated that 0.26% of the enzyme preparation is preloaded with an NTP donor. The salient findings were that replacing ATP with either GTP, CTP, UTP, or dATP resulted in 98% phosphorylation of the acceptor RNA strand (Figure 1B). We conclude that the *Cth*Pnkp kinase does not require an adenine nucleobase or ribose sugar in the phosphate donor substrate. To query whether a nucleoside moiety was even necessary, we tested kinase activity in a reaction mixture containing 100 μM inorganic tripolyphosphate in lieu of an NTP. We found that tripolyphosphate did not support the kinase reaction (not shown). A mixing experiment showed that 100 μM tripolyphosphate did not inhibit kinase activity in the presence of 100 μM ATP (not shown). These results suggest that a nucleoside moiety is needed for occupancy of the donor site on the kinase.

We gauged the kinetics of the RNA phosphorylation reaction under conditions of enzyme excess, whereby reactions containing 50 nM $_{HO}$RNAp and 100 μM ATP were initiated by adding 0.25, 0.5, 1.0, or 2.0 μM kinase. The kinetic profiles are shown in Figure 1C, with each datum being the average of three independent experiments ± SEM. The data were fit by nonlinear regression to a one-phase association in Prism; the observed rate constants increased with enzyme concentration (k_{obs} values of 0.23 ± 0.018, 0.53 ± 0.006, 1.17 ± 0.021, and 2.17 ± 0.082 min^{-1} at 0.25, 0.5, 1.0, and 2.0 μM kinase, respectively), signifying that kinase•$_{HO}$RNAp association, rather than reaction chemistry, was rate-limiting under these conditions (i.e., in which the concentration of the 5′-OH acceptor strand was low).

NDP Acceptor Specificity of the Reverse Kinase Reaction. The polynucleotide kinase enzymes of bacteriophages T4, KVP40, Omega, and Cjw1 and of the archaeon *Pyrococcus horikoshii* can transfer a polynucleotide 5′-PO_4 to ADP to form ATP and a 5′-OH polynucleotide.[21−23] To assess if *Cth*Pnkp can also catalyze reversal of the kinase reaction, we incubated the enzyme with 5′-^{32}P-labeled 15-mer DNA and Mg^{2+} in the presence of 100 μM ADP. This resulted in the formation of a ^{32}P-ATP product that was resolved from the oligonucleotide by PEI-cellulose TLC (Figure 2A); 88% of the input polynucleotide 5′-PO_4 was converted to ATP; omission of the ADP acceptor resulted in no release of label from the ^{32}P-DNA. The finding that 100 μM GDP, CDP, UDP, and dADP also served as acceptors for the reverse kinase reaction, resulting in the formation of ^{32}P-labeled GTP, CTP, UTP, and dATP, respectively (Figure 2A), fortified the conclusions from the experiments in Figure 1B that the bacterial polynucleotide kinase is neither nucleobase- nor sugar-specific with respect to its nucleotide substrate. No label was released in the presence of 100 μM inorganic pyrophosphate (not shown).

Phosphoryl transfer from ^{32}P-DNA to NDPs to form ^{32}P-NTPs displayed a hyperbolic dependence on NDP concentration, with apparent K_m values of 18 ± 1.5 μM ADP, 18 ± 2.2 μM GDP, 32 ± 5.0 μM CDP, 44 ± 6.8 μM dATP, and 64 ± 6.2 μM UDP (Figure 2B). The kinetics of the reverse kinase reaction were analyzed under conditions of enzyme excess (0.1 μM pDNA, 100 μM ADP, and 0.25, 0.5, 1.0, or 2.0 μM kinase). The kinetic profiles are shown in Figure 2C. The data were fit by nonlinear regression to a one-phase association in Prism; the k_{obs} values increased with kinase concentration (0.17 ± 0.004, 0.53 ± 0.018, 0.83 ± 0.043, and 1.57 ± 0.05 min^{-1} at 0.25, 0.5, 1.0, and 2.0 μM kinase, respectively), signifying that kinase•pDNA association, rather than reaction chemistry, was rate-limiting.

Dependence of Kinase Activity on the Concentration of the 5′-OH Polynucleotide. The above findings that the rate constants for the forward and reverse kinase reactions performed at 0.05 or 0.1 μM polynucleotide were proportional to kinase concentration even at enzyme excess prompted us to assess the affinity of the kinase for the 15-mer 5′-OH DNA phosphoacceptor under conditions of substrate excess. The extent of DNA phosphorylation during a 2 min reaction with 100 μM [γ^{32}P]ATP is plotted as a function of $_{HO}$DNA concentration in Figure 3. Nonlinear regression fitting of the data to the Michaelis−Menten equation yielded a K_m of 2.8 ± 0.4 μM for the $_{HO}$DNA phosphoacceptor and a k_{cat} of 4.3 ± 0.2 min^{-1}.

Structures of the Kinase in Complexes with GTP, CTP, UTP, and dATP. To gain further insights to phosphate donor selection, we crystallized the kinase in the presence of 10 mM $MgCl_2$ plus 2 mM GTP, CTP, UTP, or dATP. (By contrast, we were unable to grow crystals of the kinase in the presence of 10 mM $MgCl_2$ plus 2 mM inorganic tripolyphosphate, which is not an effective phosphate donor for the kinase reaction.) The refinement statistics and model contents of the kinase•GTP•Mg^{2+}, kinase•UTP•Mg^{2+}, kinase•dATP•Mg^{2+}, and kinase•CTP•Mg^{2+} structures at 2.14, 2.03, 2.02, and 2.49 Å resolution, respectively, are provided in Table 1.

Stereoviews of the $2F_o-F_c$ maps for the NTP•Mg^{2+} ligands in the refined model are shown in Figure 4. They reveal distinctive electron density over the nucleobase that discriminates adenine from guanine (via the exocyclic N2 atom of guanine) and the larger purines from the two pyrimidines. The

dx.doi.org/10.1021/bi400412x | *Biochemistry* 2013, 52, 4734−4743

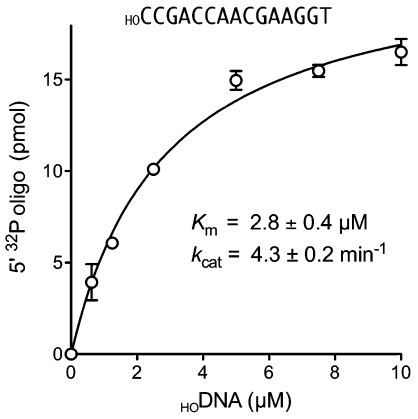

Figure 3. Dependence of kinase activity on 5′-OH polynucleotide concentration. Reaction mixtures (10 μL) containing 50 mM Tris-HCl (pH 7.0), 10 mM $MgCl_2$, 5 mM DTT, 100 μM [γ^{32}P]ATP, 0.25 μM kinase, and 15-mer 5′-OH DNA oligonucleotide phosphoacceptor ($_{HO}$CCGACCAACGAAGGT) as specified were incubated for 2 min at 45 °C. The reactions were initiated by adding kinase to prewarmed reaction mixtures and quenched with formamide and EDTA. The extents of DNA phosphorylation are plotted as a function of $_{HO}$DNA concentration. Each datum is the average of three $_{HO}$DNA titration experiments ± SEM. Nonlinear regression curve fitting to the Michaelis–Menten equation was performed in Prism.

guanosine and adenosine nucleosides are in an *anti* conformation (Figure 4, left panels), as are the uridine and cytidine nucleosides, as gauged by the density over their respective pyrimidine O2 atoms (Figure 4, right panels). The ribose O2′ atoms in the GTP, UTP, and CTP ligands are evident in the electron density maps; as expected, there is no density for an O2′ atom in the dATP ligand (Figure 4). Each nucleobase makes a π–cation stack on the Arg116 side chain.

The tertiary structure of the crystallized kinase was virtually identical when bound to ATP, GTP, UTP, CTP, or dATP, with rmsd values of 0.13 to 0.32 Å over 171 Cα atoms. The NTP donor sites of all five kinase•NTP•Mg^{2+} structures are superimposed in a stereoview in Figure 5. The triphosphate moieties of the NTPs are virtually identical in position and conformation. The Thr23 hydroxyl donates a hydrogen bond to the NTP α phosphates. The Lys21 side chain makes a bifurcated ionic interaction with the NTP β and γ phosphates, and the NTP γ phosphates are engaged by Arg120. Ser22 coordinates the Mg^{2+} ion. There is virtually no positional variation in the Lys21, Ser22, Thr23, and Arg120 side chains in the kinase•NTP structures (Figure 5). The Arg123 side chain near the NTP γ phosphates does vary with respect to the position of its terminal guanidinium moiety. The nucleobases vary slightly (e.g., guanine is shifted counterclockwise relative to adenine in the view in Figure 5), but they are all coplanar and stacked over the Arg116 side chain. There are no additional enzymic contacts to the nucleoside in any of the kinase•NTP structures.

Mutational Analysis. Previously, we initiated a structure-guided mutational analysis of the ATP phosphate donor site of the kinase by testing the effects of alanine substitutions in the context of the *Cth*Pnkp-(1–425) protein, comprising the kinase and phosphatase catalytic domains.[14] The wild-type and mutant preparations were assayed for kinase activity in reaction mixtures containing an amount of wild-type protein that sufficed for near-quantitative radiolabeling of the input 5′-OH DNA oligonucleotide acceptor in the presence of 100 μM [γ^{32}P]ATP. We chose to conduct the screening assays in this fashion in order to highlight the most severe mutational effects on catalysis. We found that the kinase activity was ablated by subtraction of Lys21, whereas elimination of the Ser22 hydroxyl group reduced activity by an order of magnitude. Kinase activity was abolished by alanine substitution for Asp38, consistent with its postulated role in orienting and activating the polynucleotide 5′-OH nucleophile.[14] By contrast, replacing lid residue Arg116 with alanine had little impact on the extent of DNA labeling. Mutating lid residue Arg120 to alanine also had little impact.

The relatively benign effects of subtracting the lid arginine residues was surprising to us and suggested that the contributions of their individual contacts with the ATP phosphate donor might either be functionally redundant or masked by the assay conditions employed (saturating enzyme, saturating ATP). For example, the contact of Arg120 with the ATP γ phosphate might be redundant with the contacts to the γ phosphate made by Arg123 (Figure 1A). To address this issue, we made single R120A and R123A changes and a double R120A–R123A mutation in the context of *Cth*Pnkp-(1–170). We assayed the extent of label transfer from 100 μM [γ^{32}P]ATP to 6 μM 15-mer $_{HO}$DNA acceptor as a function of input protein (Figure 6). Specific activities of the wild-type and mutant kinases were derived by linear regression curve fitting in Prism and then normalized to the wild-type activity (defined as 100%). The R120A and R123A mutants were 42 and 77% as active as wild-type, respectively. The R120A–R123A double mutant was 13% as active as wild-type (Figure 6), suggesting that the lid Arg120 and Arg123 side chains do indeed make functionally redundant contacts to the γ phosphate oxygens.

It is noteworthy that the effects of singly subtracting the lid arginines that contact the γ phosphate on the *Cth*Pnkp kinase activity are much milder than those observed for other homologous P-loop phosphotransferases. A single R126A change in the lid of bacteriophage T4 Pnkp (corresponding to the R120A mutation in *Cth*Pnkp) reduced kinase specific activity to 3% of the wild-type value.[24] Changing the equivalent Arg132 residue of chicken muscle adenylate kinase (a prototypal nucleoside 5′ monophosphate kinase[25]) to methionine reduced k_{cat} by a factor of 8000 without affecting K_m for the ATP phosphate donor.[26,27] Replacing chicken adenylate kinase Arg138 (corresponding to Arg123 in *Cth*Pnkp) with methionine was even more deleterious, eliciting a 13000-fold decrement in k_{cat} and increasing K_m for the AMP phosphate acceptor by 20-fold.[26,28] By contrast, the R123A change in *Cth*Pnkp has little impact on kinase specificity activity (Figure 6). The disparate effects of the loss of this structurally homologous distal lid arginine might reflect the different chemistries of the respective kinase reactions, whereby, in adenylate kinase, the distal lid arginine contacts the AMP phosphate nucleophile that attacks the ATP γ phosphorus.[29,30] By contrast, the 5′-OH nucleophile in the polynucleotide kinase reaction is coordinated and activated by an essential aspartate: Asp38 in *Cth*Pnkp and Asp35 in T4 Pnkp.[14,31–33]

The *Cth*Pnkp-(1–170) Arg116A mutant was 83% as active as the wild-type kinase (Figure 6). Given the role of the Arg116 guanidinium as a stacking platform for the NTP nucleobase, we queried whether its loss had any impact on the K_m for ATP. Wild-type and R116A kinase preparations purified to apparent homogeneity through a gel-filtration step were assayed for label transfer from [γ^{32}P]ATP to the a 15-mer $_{HO}$DNA acceptor under conditions of substrate excess (0.25 μM kinase; 10 μM

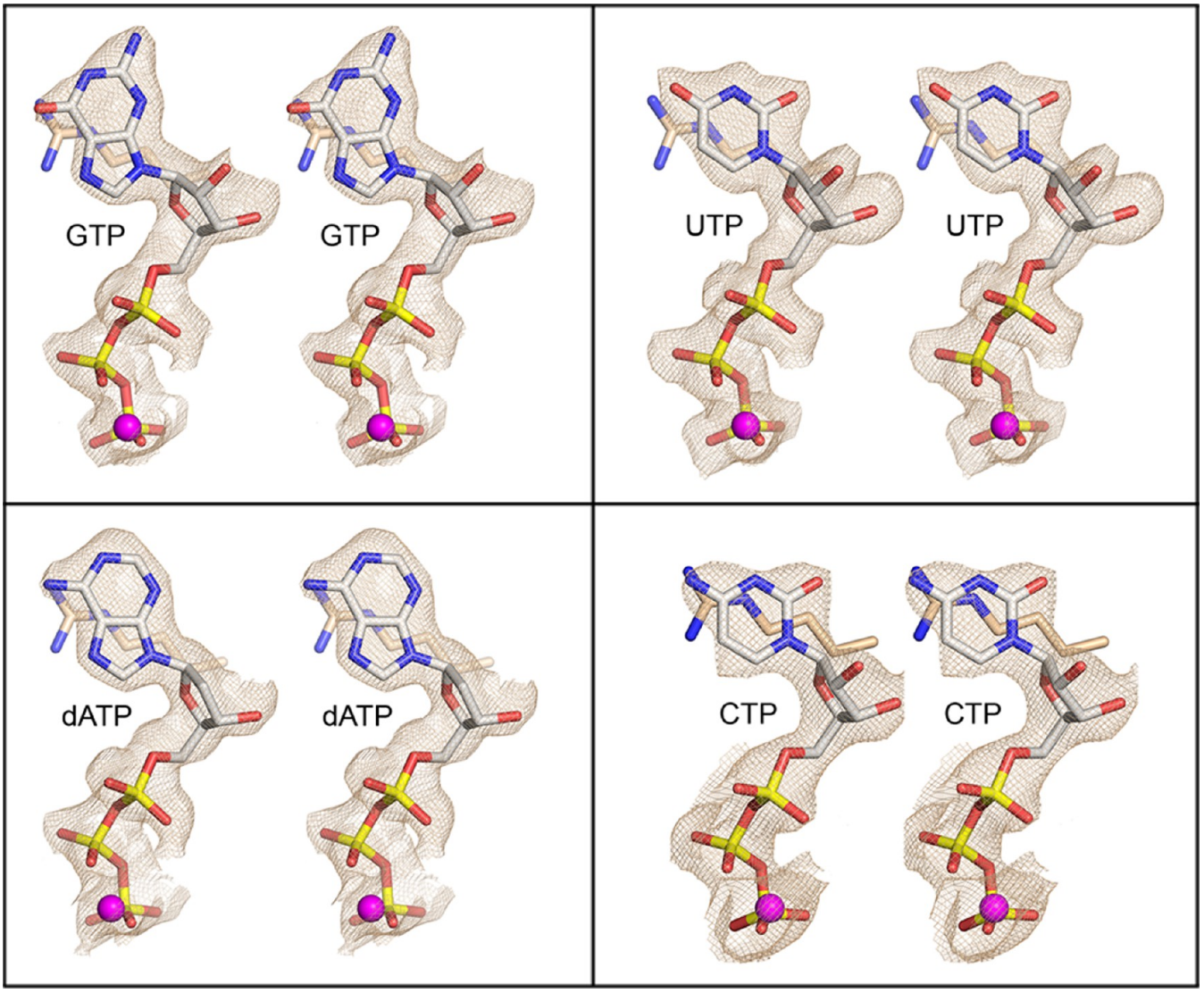

Figure 4. Nucleotide electron density in the kinase•NTP•Mg^{2+} complexes. Stereoviews of the $2F_o-F_c$ electron density maps of the nucleotides in the kinase•GTP•Mg^{2+}, kinase•dATP•Mg^{2+}, kinase•UTP•Mg^{2+}, and kinase•CTP•Mg^{2+} complexes, contoured at 1.5σ. The NTPs are shown as stick models with gray carbons. Magnesium ions are depicted as magenta spheres. The Arg116 side chain underlying the nucleobase is shown as a stick model with beige carbons.

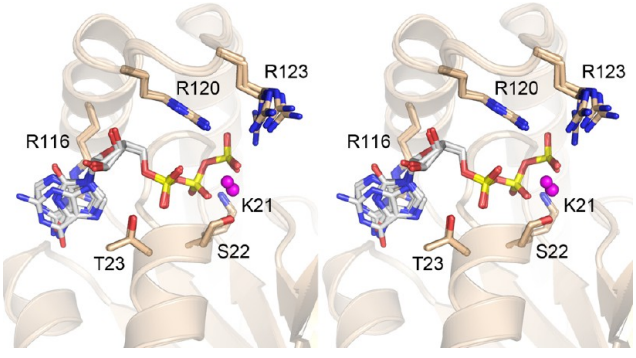

Figure 5. Superposition of five kinase•NTP structures. A stereoview of the superimposed kinase•NTP•Mg^{2+} complexes with ATP (from pdb 4GP7), GTP, CTP, UTP, and dATP. NTPs in the phosphate donor site are shown as stick models with gray carbons. Magnesium ions are depicted as magenta spheres. Selected Pnkp side chains are shown as stick models with beige carbons.

$_{HO}$DNA). The extents of DNA phosphorylation during a 2 min reaction are plotted as a function of [γ^{32}P]ATP concentration in Figure 7. Nonlinear regression fitting of the data to the Michaelis–Menten equation yielded steady-state parameters for the wild-type kinase (K_m = 4.0 ± 0.7 μM ATP; k_{cat} = 4.6 ± 0.2 min^{-1}) and R116A mutant (K_m = 40 ± 6 μM ATP; k_{cat} = 4.4 ± 0.3 min^{-1}). These results signify that the π–cation interaction of Arg116 with the adenine nucleobase enhances affinity for the ATP phosphate donor by 10-fold but has little effect on the rate of phosphoryl transfer chemistry.

■ DISCUSSION

The present study provides new insights to the mechanism by which *Cth*Pnkp heals 5′-OH ends, especially the contributions of the arginine residues that emanate from the lid that overlies the NTP phosphate donor site. Prompted by the paucity of enzymic contacts to the nucleoside of ATP in our initial crystal structure of the kinase, we interrogated the NTP specificity of *Cth*Pnkp. We found that the kinase utilizes any of the NTPs

dx.doi.org/10.1021/bi400412x | *Biochemistry* 2013, 52, 4734–4743

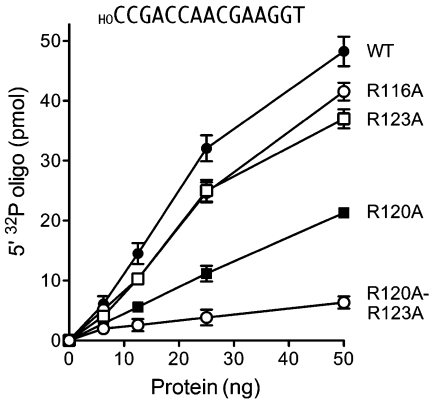

Figure 6. Structure-guided mutagenesis. Kinase reactions were performed as described in Experimental Procedures. The reaction mixtures included 100 μM [γ^{32}P]ATP, 60 pmol of a 15-mer 5′-OH DNA oligonucleotide ($_{HO}$CCGACCAACGAAGGT), and wild-type or mutant kinase as indicated. The extents of DNA phosphorylation are plotted as a function of input protein. Each datum is the average of three titration experiments ± SEM.

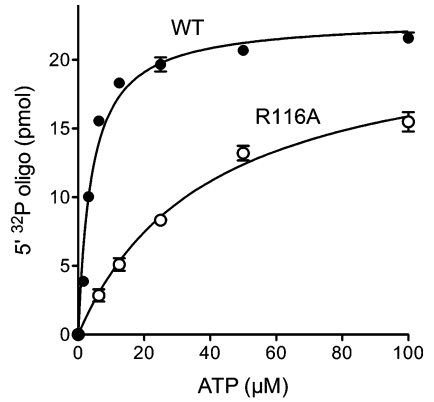

Figure 7. Steady-state kinetics. Reaction mixtures (10 μL) containing 50 mM Tris-HCl (pH 7.0), 10 mM $MgCl_2$, 5 mM DTT, 100 pmol of a 15-mer 5′-OH DNA oligonucleotide phosphoacceptor ($_{HO}$CCGACCAACGAAGGT), 0.25 μM wild-type or R116A kinase, and [γ^{32}P]ATP as specified were incubated for 2 min at 45 °C. The reactions were initiated by adding kinase to prewarmed reaction mixtures and quenched with formamide and EDTA. The extents of DNA phosphorylation are plotted as a function of ATP concentration. Each datum is the average of three ATP titration experiments ± SEM. Nonlinear regression curve fitting to the Michaelis–Menten equation was performed in Prism.

tested as donor substrates for phosphorylation of a polynucleotide 5′-OH end in the forward kinase reaction. Moreover, the kinase uses any of the NDPs tested as phosphate acceptors in the reverse kinase reaction, in which a polynucleotide 5′-PO_4 is transferred to an NDP to generate the cognate NTP. The apparent K_m values for rNDP acceptors in the reverse reaction varied over a ~3-fold range, with GDP and ADP being superior to CDP and UDP. (This could reflect the size of the nucleobase π systems available for interaction with Arg116.) Whereas the *Cth*Pnkp kinase is not stringently specific for the nucleobase (or the ribose sugar), the enzyme requires a nucleoside, insofar as tripolyphosphate and pyrophosphate do not serve as donor and acceptor in the forward and reverse kinase reactions, respectively.

We focused on the role of Arg116, the sole contact between the kinase and the nucleobase of the NTP phosphate donor. By solving new crystal structures of the kinase in complexes with GTP, dATP, CTP, and UTP, we showed that the purine and pyrimidine nucleobases are in *anti* conformation and are coplanar in a π–cation stack over the Arg116 guanidinium. Subtracting this interaction by replacing Arg116 with alanine caused a 10-fold increase in K_m for ATP but had little effect on k_{cat}. These findings illuminate the basis for nonspecific donor nucleotide utilization by a P-loop phosphotransferase.

It is worthwhile to compare the phosphate donor specificity of *Cth*Pnkp kinase to other polynucleotide kinases and P-loop phosphotransferases/phosphohydrolases. The kinase domains of bacteriophage T4 Pnkp and *Cth*Pnkp are structurally homologous. The crystal structure[34] of T4 kinase bound to ADP revealed that the adenine base makes a π–cation stack over Arg122, which is the counterpart of Arg116 in *Cth*Pnkp. This is the sole contact between T4 Pnkp and the adenosine nucleoside, presumably explaining why T4 kinase catalyzes reversible transfer of the γ phosphate from any NTP to a polynucleotide 5′-OH end. The effects of subtracting Arg122 on the affinity of T4 Pnkp for the nucleotide substrates have not been reported.

Plant tRNA ligase AtRNL has a central kinase domain that uses any NTP or dATP as a phosphate donor for converting 5′-OH RNA ends to 5′-PO_4 ends.[35] Although there is no structure available for AtRNL, its kinase module belongs to the P-loop superfamily, and it includes a putative counterpart of the lid: ^{800}RVLQR^{804}, corresponding to ^{116}RNKNR^{120} in *Cth*Pnkp.[36] By contrast, yeast tRNA ligase Trl1 strongly prefers GTP over ATP as the phosphate donor for its 5′-OH kinase reaction.[37] Given that Trl1 also has a lid counterpart (^{507}RNSKR^{511}) that includes the nucleobase-stacking arginine, we presume that the Trl1 kinase (unlike the *Cth* and T4 kinases) does make additional contacts with the guanine base that account for this specificity.

Mammalian Pnkp is specific for 5′-OH DNA as the phosphoacceptor in the kinase reaction. It also catalyzes the reverse kinase reaction with a 5′-PO_4 DNA donor and various rNDPs or dNDPs (but not PP_i) as phosphate acceptors.[38] The crystal structure of mammalian Pnkp with ADP•Mn^{2+} in the kinase active site is available.[39] When superimposed on the *Cth*Pnkp kinase•ADP•Mg^{2+} structure (pdb 4GP6), the ADP•metal ligands are virtually identical in position and conformation and in their key contacts with the P-loop lysine, serine, and threonine side chains. Yet, mammalian kinase does not have an equivalent of the *Cth*Pnkp kinase Arg116 residue (it being asparagine instead), and there is no π–cation or π–π interaction of the enzyme with the adenine nucleobase. Rather, the mammalian kinase forms hydrogen bonds from a main-chain carbonyl to adenine N6 and from a main-chain NH to adenine N1.[39] Conversely, there are no counterparts of the mammalian kinase adenine-binding elements in *Cth*Pnkp. The mammalian Pnkp structure suggests that mammalian kinase ought to be selective for adenine nucleotides, which runs counter to the earlier report that the enzyme uses multiple NDPs in the reverse reaction. Finer biochemical analysis of the NTP donor specificity of mammalian DNA kinase, coupled with attempts to cocrystallize mammalian Pnkp with alternative NTPs or NDPs in the kinase active site, could clarify the issue.

Archaeal and human Clp1 are homologous 5′-OH RNA kinases implicated in RNA repair.[23,40,41] The archaeal Clp1 kinase reaction is reversible, and any rNDP suffices as the phosphoacceptor substrate.[23] By contrast, human Clp1 favors ATP over GTP as the phosphate donor.[40] The yeast Clp1

dx.doi.org/10.1021/bi400412x | *Biochemistry* 2013, 52, 4734–4743

homologue binds ATP•Mg^{2+} at its P-loop, yet yeast Clp1 is devoid of kinase or ATPase activity.[42] On the basis of the crystal structure of a yeast Clp1•ATP•Mg^{2+} complex,[42] one predicts that archaeal and human Clp1 kinase lacks a counterpart of the lid module found in *Cth*Pnkp, T4 Pnkp, and mammalian Pnkp. Whereas *Cth*Pnkp and T4 Pnkp have an open nucleoside site on the enzyme surface, yeast Clp1 envelops the nucleobase and ribose within a pocket formed by an accessory domain not found in the bacterial and phage kinases. Gauging whether the same nucleoside binding mode applies to the kinase-active human and archaeal Clp1 proteins must await their structure determination.

Adenylate kinases have a lid domain with a conserved RxxxR motif that engages the ATP substrate. The proximal arginine in the lid motif (Arg119 in *E. coli* adenylate kinase and Arg128 in yeast adenylate kinase, corresponding to Arg116 in *Cth*Pnkp) makes a π−cation stack on the adenine nucleobase of the phosphate donor.[29,30] Preference for ATP as the donor in the adenylate kinase reaction is thought to be conferred by a single hydrogen bond from the adenine N7 atom to a main-chain carbonyl oxygen of the enzyme.[25,29,30]

The P-loop ATPase *E. coli* UvrD exemplifies the superfamily I clade of DNA helicases. (UvrD is a phosphohydrolase rather than a phosphotransferase.) Crystal structures of UvrD with adenosine nucleotides in the active site highlight a combination of nucleobase-unspecific and adenine-specific enzymic contacts.[16] To wit, the adenine base is sandwiched within a cation−π−π stack with an arginine guanidinium on one side of the adenine and a tyrosine on the other. A glutamine side chain makes two hydrogen bonds to the adenine ring nitrogens: one from Gln-Nε to adenine N7 and another from Gln-Oε to adenine N6.[16] This glutamine is conserved in many ATPase/dATPase helicases; in the case of mycobacterial UvrD1, the glutamine acts as a substrate filter, such that when it is replaced by alanine UvrD1 gains a new activity as a UTPase/TTPase.[17]

In conclusion, diverse P-loop phosphotransferases with different NTP donor and 5′-OH acceptor specificities have evolved to contend with the 5′ end-healing problem during RNA and DNA repair. Whereas some polynucleotide kinases are fastidious with respect to the nucleobase or the pentose sugar of the NTP substrate, others are not. The arginine π−cation interaction with all nucleobases seen in our suite of *Cth*Pnkp•NTP•Mg^{2+} structures is a seemingly effective strategy to enhance NTP affinity without imposing stringent NTP selectivity.

■ ASSOCIATED CONTENT

Accession Codes

The coordinates for the refined models of kinase•GTP•Mg^{2+}, kinase•CTP•Mg^{2+}, kinase•UTP•Mg^{2+}, and kinase•dATP•Mg^{2+} have been deposited in the RCSB protein structure database (PDB ID codes 4JSY, 4JT2, 4JST, and 4JT4).

■ AUTHOR INFORMATION

Corresponding Author

*Phone: 212-639-7145. E-mail: s-shuman@ski.mskcc.org.

Funding

This research was supported by NIH Grant GM42498.

Notes

The authors declare no competing financial interest.

■ ACKNOWLEDGMENTS

We thank NSLS staff members Annie Heroux and Neil Whalen for their assistance with data collection. This research was supported by NIH Grant GM42498. S.S. is an American Cancer Society Research Professor.

■ REFERENCES

(1) Nandakumar, J., Schwer, B., Schaffrath, R., and Shuman, S. (2008) RNA repair: an antidote to cytotoxic eukaryal RNA damage. *Mol. Cell 31*, 278−286.

(2) Popow, J., Schleiffer, A., and Martinez, J. (2012) Diversity and roles of (t)RNA ligases. *Cell. Mol. Life Sci. 69*, 2657−2670.

(3) Martins, A., and Shuman, S. (2005) An end-healing enzyme from *Clostridium thermocellum* with 5′ kinase, 2′,3′ phosphatase, and adenylyltransferase activities. *RNA 11*, 1271−1280.

(4) Chan, C. M., Zhou, C., and Huang, R. H. (2009) Reconstituting bacterial RNA repair and modification in vitro. *Science 326*, 247.

(5) Jain, R., and Shuman, S. (2010) Bacterial Hen1 is a 3′ terminal RNA ribose 2′*O*-methyltransferase component of a bacterial RNA repair cassette. *RNA 16*, 316−323.

(6) Keppetipola, N., and Shuman, S. (2006) Mechanism of the phosphatase component of *Clostridium thermocellum* polynucleotide kinase-phosphatase. *RNA 12*, 73−82.

(7) Keppetipola, N., and Shuman, S. (2006) Distinct enzymic functional groups are required for the phosphomonoesterase and phosphodiesterase activities of *Clostridium thermocellum* polynucleotide kinase/phosphatase. *J. Biol. Chem. 281*, 19251−19259.

(8) Keppetipola, N., and Shuman, S. (2007) Characterization of the 2′,3′ cyclic phosphodiesterase activities of *Clostridium thermocellum* polynucleotide kinase-phosphatase and bacteriophage λ phosphatase. *Nucleic Acids Res. 35*, 7721−7732.

(9) Keppetipola, N., Nandakumar, J., and Shuman, S. (2007) Reprogramming the tRNA splicing activity of a bacterial RNA repair enzyme. *Nucleic Acids Res. 35*, 3624−3630.

(10) Smith, P., Wang, L. K., Nair, P. A., and Shuman, S. (2012) The adenylyltransferase domain of bacterial Pnkp defines a unique RNA ligase family. *Proc. Natl. Acad. Sci. U.S.A. 109*, 2296−2301.

(11) Wang, P., Chan, C. M., Christensen, D., Zhang, C., Selvadurai, K., and Huang, R. H. (2012) Molecular basis of bacterial protein Hen1 activating the ligase activity of bacterial protein Pnkp for RNA repair. *Proc Natl. Acad. Sci. U.S.A. 109*, 13248−13253.

(12) Chan, C. M., Zhou, C., Brunzelle, J. S., and Huang, R. H. (2009) Structural and biochemical insights into 2′-*O*-methylation at the 3′-terminal nucleotide of RNA by Hen1. *Proc. Natl. Acad. Sci. U.S.A. 106*, 17699−17704.

(13) Jain, R., and Shuman, S. (2011) Active site mapping and substrate specificity of bacterial Hen1, a manganese-dependent 3′ terminal RNA ribose 2′*O*-methyltransferase. *RNA 17*, 429−438.

(14) Wang, L. K., Das, U., Smith, P., and Shuman, S. (2012) Structure and mechanism of the polynucleotide kinase component of the bacterial Pnkp-Hen1 RNA repair system. *RNA 18*, 2277−2286.

(15) Wang, L. K., Smith, P., and Shuman, S. (2013) Structure and mechanism of the 2′,3′ phosphatase component of the bacterial Pnkp-Hen1 RNA repair system. *Nucleic Acids Res.*,.

(16) Lee, J. Y., and Yang, W. (2006) UvrD helicase unwinds DNA one base pair at a time by a two-part power stroke. *Cell 127*, 1349−1360.

(17) Sinha, K. M., Glickman, M. S., and Shuman, S. (2009) Mutational analysis of Mycobacterium UvrD1 identifies functional groups required for ATP hydrolysis, DNA unwinding, and chemomechanical coupling. *Biochemistry 48*, 4019−4030.

(18) Emsley, P., and Cowtan, K. (2004) Coot: model-building tools for molecular graphics. *Acta Crystallogr. D60*, 2126−2132.

(19) Adams, P. D., Grosse-Kunstleve, R. W., Hung, L. W., Ioerger, T. R., McCoy, A. J., Moriarty, N. W., Read, R. J., Sacchettini, J. C., Sauter, N. K., and Terwilliger, T. C. (2002) PHENIX: building new software for automated crystallographic structure determination. *Acta Crystallogr. D58*, 1948−1954.

(20) Das, U., and Shuman, S. (2013) Mechanism of RNA 2′,3′-cyclic phosphate end-healing by T4 polynucleotide kinase-phosphatase. *Nucleic Acids Res. 41*, 355−365.
(21) van de Sande, J. H., Kleppe, K., and Khorana, H. G. (1973) Reversal of bacteriophage T4 induced polynucleotide kinase action. *Biochemistry 12*, 5050−5055.
(22) Zhu, H., Yin, S., and Shuman, S. (2004) Characterization of polynucleotide kinase/phosphatase enzymes from mycobacteriophages Omega and Cjw1 and vibriophage KVP40. *J. Biol. Chem. 279*, 26358−26369.
(23) Jain, R., and Shuman, S. (2009) Characterization of a thermostable archaeal polynucleotide kinase homologous to human Clp1. *RNA 15*, 923−931.
(24) Wang, L. K., and Shuman, S. (2002) Mutational analysis defines the 5′ kinase and 3′ phosphatase active sites of T4 polynucleotide kinase. *Nucleic Acids Res. 30*, 1073−1080.
(25) Yan, H., and Tsai, M. D. (1999) Nucleoside monophosphate kinases: structure, mechanism, and substrate specificity. *Adv. Enzymol. Relat. Areas Mol. Biol. 73*, 103−134.
(26) Tsai, M. D., and Yan, H. (1991) Mechanism of adenylate kinase: site-directed mutagenesis versus X-ray and NMR. *Biochemistry 30*, 6806−6818.
(27) Dahnke, T., Shi, Z., Yan, H., Jiang, R. T., and Tsai, M. D. (1992) Mechanism of adenylate kinase. Structural and functional roles of the conserved arginine-97 and arginine-132. *Biochemistry 31*, 6318−6328.
(28) Yan, H., Shi, Z., and Tsai, M. D. (1990) Mechanism of adenylate kinase. Structural and functional demonstration of arginine-138 as a key catalytic residue that cannot be replaced by lysine. *Biochemistry 29*, 6385−6392.
(29) Müller, C. W., and Schulz, G. E. (1992) Structure of the complex between adenylate kinase from *Escherichia coli* and the inhibitor Ap_5A refined at 1.9 Å resolution: a model for a catalytic transition state. *J. Mol. Biol. 224*, 159−177.
(30) Abele, U., and Schulz, G. E. (1995) High-resolution structures of adenylate kinase from yeast ligated with inhibitor Ap_5A, showing the pathway of phosphoryl transfer. *Protein Sci. 4*, 1262−1271.
(31) Wang, L. K., and Shuman, S. (2001) Domain structure and mutational analysis of T4 polynucleotide kinase. *J. Biol. Chem. 276*, 26868−26874.
(32) Wang, L. K., Lima, C. D., and Shuman, S. (2002) Structure and mechanism of T4 polynucleotide kinase—an RNA repair enzyme. *EMBO J. 21*, 3873−3880.
(33) Eastberg, J. H., Pelletier, J., and Stoddard, B. L. (2004) Recognition of DNA substrates by bacteriophage T4 polynucleotide kinase. *Nucleic Acids Res. 32*, 653−660.
(34) Galburt, E. A., Pelletier, J., Wilson, G., and Stoddard, B. L. (2002) Structure of a tRNA repair enzyme and molecular biology workhorse: T4 polynucleotide kinase. *Structure 10*, 1249−1260.
(35) Remus, B. S., and Shuman, S. (2013) A kinetic framework for tRNA ligase and enforcement of a 2′-phosphate requirement for ligation highlights the design logic of an RNA repair machine. *RNA*,.
(36) Wang, L. K., Schwer, B., Englert, M., Beier, H., and Shuman, S. (2006) Structure−function analysis of the kinase-CPD domain of yeast tRNA ligase (Trl1) and requirements for complementation of tRNA splicing by a plant Trl1 homolog. *Nucleic Acids Res. 34*, 517−527.
(37) Westaway, S. K., Belford, H. G., Apostol, B. L., Abelson, J., and Greer, C. L. (1993) Novel activity of a yeast ligase deletion polypeptide: evidence for GTP-dependent tRNA splicing. *J. Biol. Chem. 268*, 2435−2443.
(38) Pheiffer, B. H., and Zimmerman, S. B. (1979) Deoxyribonucleic acid kinase from nuclei of rat liver: mechanism, reversal, and inhibitors of the reaction. *Biochemistry 18*, 2960−2963.
(39) Garces, F., Pearl, L. H., and Oliver, A. W. (2011) The structural basis for substrate recognition by mammalian polynucleotide kinase 3′ phosphatase. *Mol. Cell 44*, 385−396.
(40) Weitzer, S., and Martinez, J. (2007) The human RNA kinase hClp1 is active on 3′ transfer RNA exons and short interfering RNAs. *Nature 447*, 222−226.
(41) Ramirez, A., Shuman, S., and Schwer, B. (2008) Human RNA 5′-kinase (hClp1) can function as a tRNA splicing enzyme in vivo. *RNA 14*, 1737−1745.
(42) Noble, C. G., Beuth, B., and Taylor, I. A. (2007) Structure of a nucleotide-bound Clp1-Pcf11 polyadenylation factor. *Nucleic Acids Res. 35*, 87−99.